Mapping Greenland's mass loss in space and time

Christopher Harig[1] and Frederik J. Simons

Department of Geosciences, Princeton University, Princeton, NJ 08544

Edited by Mark H. Thiemens, University of California at San Diego, La Jolla, CA, and approved October 9, 2012 (received for review April 24, 2012)

The melting of polar ice sheets is a major contributor to global sea-level rise. Early estimates of the mass lost from the Greenland ice cap, based on satellite gravity data collected by the Gravity Recovery and Climate Experiment, have widely varied. Although the continentally and decadally averaged estimated trends have now more or less converged, to this date, there has been little clarity on the detailed spatial distribution of Greenland's mass loss and how the geographical pattern has varied on relatively shorter time scales. Here, we present a spatially and temporally resolved estimation of the ice mass change over Greenland between April of 2002 and August of 2011. Although the total mass loss trend has remained linear, actively changing areas of mass loss were concentrated on the southeastern and northwestern coasts, with ice mass in the center of Greenland steadily increasing over the decade.

spatiospectral localization | time-variable gravity | climate change | ice melt

The contribution to global sea-level rise from the melting of polar ice sheets has been a focus of intense study over the past several decades. Earth's second-largest ice sheet, Greenland, has been surveyed by a multitude of techniques. Remote-sensing observations by laser and radar altimetry and interferometric synthetic aperture radar have constrained both the overall variability in Greenland's mass balance over time (1–7) and the local mass flux of its peripheral western and eastern outlet glaciers (8–11). These measurements have shown both strong variations among seasons and strong decadal variations in the inferred mass change rates (6, 12).

Coincident with these observations since 2002, the Gravity Recovery and Climate Experiment (GRACE) dual-satellite mission has been sensing the Earth's geopotential field continuously. Many studies have used monthly averaged snapshots of the field to estimate Greenland's total mass change over the years (13–18). Such estimates of the total have varied from −100 to −250 Gt/y, although as additional data have been added, the range has tightened around an average value close to −220 Gt/y (19, 20) in the last decade. One study (18) with data to 2009 has reported accelerations in the annual mass loss of Greenland of about −30 Gt/y^2.

The spatial pattern of mass loss that can be estimated from GRACE data is much less well-constrained than its average value over large areas. Whereas traditional remote-sensing techniques actively sample discrete areas on the surface, the geopotential measurement made by GRACE at altitude integrates the signal over a broad region several hundred kilometers in diameter. In addition, because of the character of the errors in the data, it is commonly deemed necessary to employ spatial smoothing (21), which further reduces the spatial resolution. GRACE results from the first half of the 2000s showed broad mass loss along the eastern half of Greenland (13–15). Later work indicated that mass loss increased along the northwest coast of Greenland later in the decade (17, 19, 20, 22). These studies shared the technique of fitting a single linear slope to several years (usually 4–5 y) of geopotential data to examine any temporal changes in the mass flux between these intervals of time.

In this paper, we determine the spatial distribution of mass loss in Greenland over time. Our inversion method relies on a spherical basis of spatiospectrally concentrated Slepian functions (23, 24). We show its ability to resolve unprecedented geographical and temporal detail in the mass flux using gravity data alone. Extracting more of the signal contained within the noisy GRACE data products, we resolve the spatial changes in mass loss on a yearly basis with robust uncertainty estimates. With our results, we aim to settle the controversies surrounding the geographical pattern of Greenland's ice loss and establish the presence or absence of significant accelerations in the ongoing trends.

The venerable spherical harmonics constitute an orthogonal function basis for the entire sphere, making the distribution of Stokes expansion coefficients for the global gravitational geopotential the standard format for the release of the GRACE level 2 data products. These (monthly) models are currently band-limited, complete to spherical harmonic degree and order 60. When examining a restricted region, such as Greenland, the use of spherical harmonics is no longer ideal or practical: their orthogonality is lost when mere portions of the sphere are being considered. Without orthogonality of the function basis over the area of interest, estimating a regional signal becomes quite a complex operation. In addition, the unfavorable error structure of the results (24–26) renders significance testing of detailed interpretations all but impossible. To obviate these difficulties, some studies gave up intracontinental spatial resolution altogether, using averaging functions over the landmass to determine the broad total rate of mass change over time (15, 27). Other works expanded the GRACE coefficients into the space domain to estimate trends on a latitude–longitude grid and compared forward models of mass anomalies (13, 19). Still other works parameterized either the direct intersatellite range measurements (14) or the global level 2 solutions (20) into basin-scale local mass variations.

By using predefined basin shapes, basis functions that are not orthogonal, smoothing and postprocessing for error reduction, or outright spatial averaging, these now common methods make assumptions about the data or the models that limit their spatial sensitivity and potentially confuse signal and noise. We postulate that the historical lack of agreement between GRACE-based models of Greenland's mass loss is at least partly because of the failure to fully characterize the tradeoffs and uncertainties that accompany these various choices of averaging, filtering, and parameterization. The differences between estimates from various groups have dwarfed the uncertainties on the instantaneous elastic response of the substrate or the relative magnitude of viscous postglacial rebound corrections, both of which are needed to convert mass anomalies to estimates of ice mass lost due to melting. However, with poorly known portions of signal lost and noise spread to lower spherical harmonic degrees by the analysis procedures, proper accounting for the effects of data processing choices is rarely at the surface of the discussion.

Here, we bypass the commonly used filtering and averaging procedures altogether, and we use a simple estimation method based on an analysis in the spherical Slepian basis explained in

Author contributions: C.H. and F.J.S. designed research, performed research, and wrote the paper.

The authors declare no conflict of interest.

This article is a PNAS Direct Submission.

[1]To whom correspondence should be addressed. E-mail: charig@princeton.edu.

This article contains supporting information online at www.pnas.org/lookup/suppl/doi:10.1073/pnas.1206785109/-/DCSupplemental.

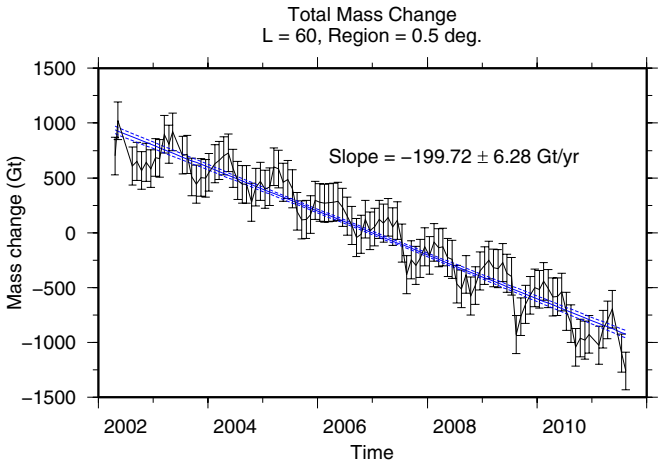

Fig. 1. Total ice mass change trend for Greenland. The solid black line is the raw GRACE monthly solution projected into the 20-term Slepian basis optimized to capture the interior of the coastlines of Greenland plus a 0.5° buffer region for a bandwidth $L = 60$ (in spherical harmonic degrees). The solid blue line is the best-fitting linear trend. The dashed blue lines represent the 2σ error envelope of this fit calculated using full covariance information estimated from the data themselves.

Model and Methods. Our methodology involves a small number of assumptions of a statistical and computational nature. Our own choices of the kind were informed by extensive simulation, and their validity was tested on numerous synthetic examples. *SI Text* has an exhaustive description of the details.

Model and Methods

The spherical Slepian basis (23) is formed by optimization to constitute a fully orthogonal, band-limited basis optimally concentrated to a region of interest (in our case, Greenland). Each Slepian function is a separate solution to an eigenvalue equation that maximizes the concentration of function energy within the specific region, and each different eigenvalue $0 \leq \lambda \leq 1$ is a measure of concentration within that region of the corresponding function. Using only those functions in the basis that have the majority of their energy concentrated within the region of interest (for example, $\lambda > 0.5$) dramatically improves the signal-to-noise ratio (24). The results experience very little influence caused by the signal originating outside the region of interest. Indeed, minimization of the well-known leakage problem is the explicit optimization objective in the construction of the Slepian basis, as it has been used in 1D signal processing for many decades (28) and in a growing number of applications in geodesy, geomagnetism, astrophysics, cosmology, and the planetary sciences. Extracting information over the full bandwidth of the solution without filtering, the spherical Slepian basis provides spatial sensitivity that is superior to the sensitivity of many other modeling methods.

We used 108 monthly GRACE Release 4 geopotential fields from the Center for Space Research, University of Texas at Austin, covering the time span from April of 2002 to August of 2011, including 5 months with data gaps. The highly variable degree-two, order-zero spherical harmonic coefficients are replaced with values from satellite laser ranging (29), and for the missing degree-one coefficients, replacement values (30) are substituted, as is by now customary. The GRACE geopotential models are transformed into surface mass density using the classical method by Wahr et al. (31); the instantaneous elastic deformation caused by current mass changes is represented and removed with degree-dependent loading Love numbers (32). The surface mass density is subsequently projected onto a Slepian basis designed to capture the region within Greenland's coastlines with the inclusion of a small buffer zone of 0.5°. We settled on the value of this buffer zone based on the simulations described in *SI Text*.

The bandwidth of the Slepian basis, $L = 60$, matches the bandwidth of the GRACE data products. We truncate the expansion at the effective dimension of the combined spatiospectral space (Greenland in space, band-limited spectrally), known as the Shannon number (23, 33). This truncation leaves only 20 target functions, each of which is an eigenmap that has its energy highly concentrated over Greenland. This sparse model space represents a significant reduction of the original spherical harmonic dimension, comprising $(L + 1)^2 = 3{,}721$ functions with expansion coefficients that are substantially influenced by noise and required estimating—or were discarded—by the alternative methods. As described, our method involves only the selection of the size of the buffer zone, the choice of bandwidth, and the number of terms in the Slepian expansion. The rationale behind our selections was validated by extensive simulation (*SI Text*), and the computer code that accompanies this paper allows the reader to reproduce the results, with modified parameter settings if such modification should be desirable.

The viscous, long-term, geopotential response of the solid Earth caused by past loading by ice caps is accounted for by subtracting from the results the postglacial rebound model by Paulson et al. (34) after projecting the latter onto the same Slepian basis as used for the GRACE-derived geopotential coefficients. The total mass over the region, relative to a 9-y mean (Fig. 1), is then calculated by integrating each function over the region, scaling by its corresponding expansion coefficient and summing over the 20 functions in the basis set. We estimate measurement error by fitting a linear trend and a harmonic with a period of 1 y to each of the Slepian coefficient time series and generating a covariance matrix from the

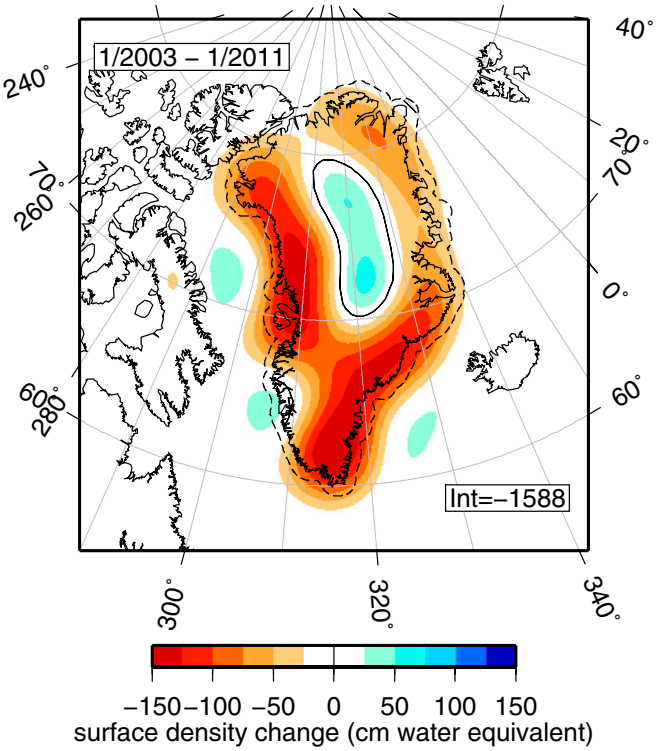

Fig. 2. Geographical pattern of the ice mass change over Greenland averaged for the period between January of 2003 and January of 2011. The map is the result of the combination of signal estimates conducted on individual time series of Slepian function expansion coefficients. The integral value (Int) for the entire epoch is shown in gigatons. The 0-cm water contour is shown in black.

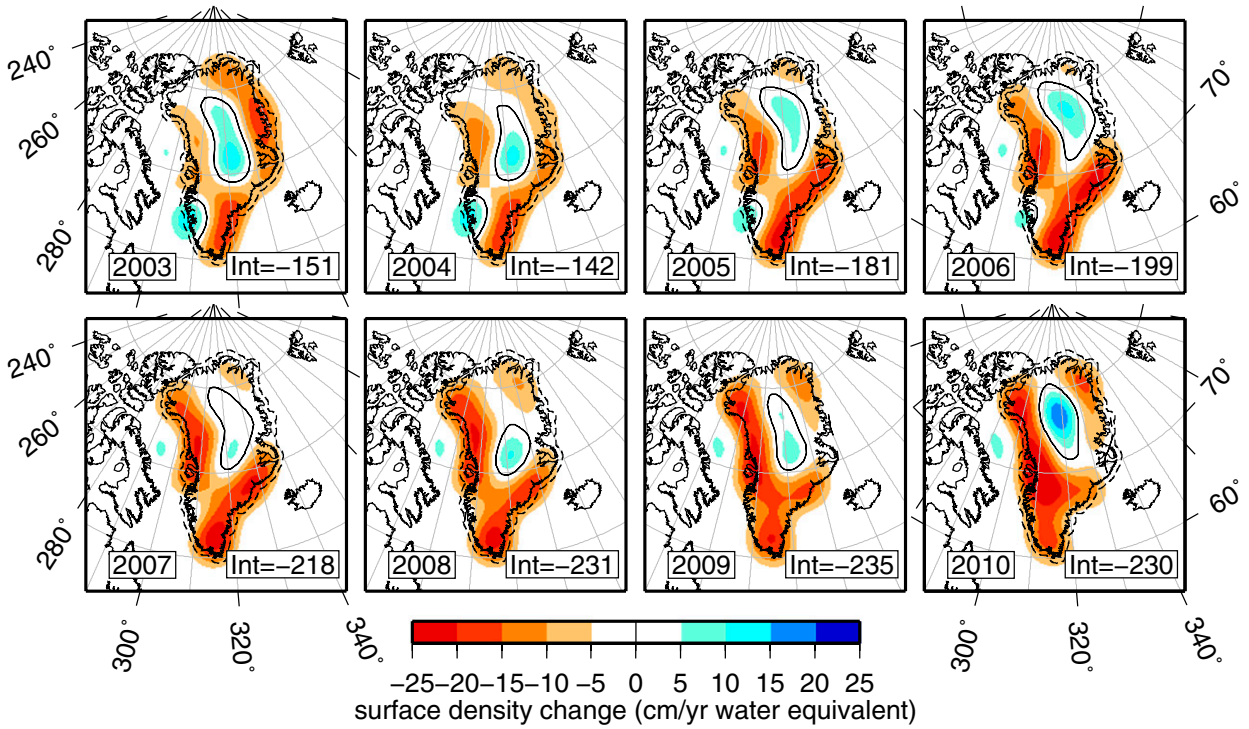

Fig. 3. Yearly resolved maps of ice mass change over Greenland from 2003 to 2010. The sum of these maps was shown in Fig. 2. For every year, we show the difference of the signal estimated between January of that year and January of the next year. The integral values (Int) of the mass change per year are shown expressed in gigatons. The 0-cm/y water contours are shown in black.

residuals. This result gives a comprehensive measure of the variance of each coefficient and their dependencies, which we extend to the uncertainty of their sum by linear error propagation. In *SI Text*, we illustrate how critical the knowledge of the covariance is for the interpretation and how different the fully nondiagonal covariance matrix is from the calibrated errors distributed as part of the GRACE data products and from errors approximately estimated using uncorrelated assumptions.

Results and Discussion

The total ice mass change (Fig. 1) shows a clear trend as well as an annual variation. The error envelope for the fit is shown with dashed lines. The overall trend is very well-determined, because with almost a decade of data, the analysis covers many seasonal cycles, which can vary strongly between years. The best-fitting linear trend covering all 108 months finds the ice mass change rate over our whole region to be -199.7 ± 6.3 Gt/y. The 2σ uncertainty on the trend derives from the covariance matrix that we estimated by the procedure described in *Model and Methods*. The uncertainty quoted does not include the uncertainty in the postglacial rebound correction, but this uncertainty could be added to the uncertainty of the trend if so desired. Many of the GRACE-based studies of Greenland use the rebound model (34), and therefore, comparisons remain straightforward. Fitting an additional quadratic (and potentially, higher-order terms, as explained in *SI Text*), we find the acceleration of mass loss to be a modest -8.68 ± 4.1 Gt/y^2.

Several recent results of the average mass trend measured from GRACE data have been near −220 Gt/y (18–20), although estimates have ranged as low as -161 ± 35 Gt/y (35). Estimates from other measurement techniques have recently been higher [e.g., -260 ± 53 Gt/y derived from surface mass balance calculations (36) or -237 ± 25 Gt/y from altimetry data (37)]. On this subject, our results are in general agreement with the most recent GRACE studies, but in obtaining them, we have relied on fewer processing steps by the judicious choice of basis, as described above. A reestimation of the trends up to the year 2006, in which three studies appeared with much variability in the conclusions (13–15), reconciles the results as nearly falling within each other's uncertainties when evaluated according to our method. We conclude that the discrepancies in the early literature were more a matter of statistics rather than physics or data selection.

Using an extension of our approach to estimate the average mass trend, we are able to measure the spatial pattern of mass change and how it changes with time. To each of our 20 Slepian function expansion coefficient time series, we have fit a first-, second-, or third-order polynomial, depending on whether each additional term passed an F test for significance. This fit then becomes our new estimate for the signal. These fits embody the gradual changes over time spans of several years, and they ignore much of the variability within each year. Fig. 2 displays a map of the total mass change of the estimated signal over the 8-y period from January of 2003 to January of 2011. Because data for the month of January of 2011 are unavailable, we used a value for January 15th, 2011 interpolated from our estimated signal for this analysis, and subsequent analyses.

Two other recent GRACE studies (20, 22) have presented results of Greenland's mass loss in map form, which are in broad agreement with what we show here. Although this convergence of the literature is a tribute to the quality and longevity of the data, the degree of spatial localization that we derive from the Slepian basis methodology significantly shrinks the geographical footprint that can now be robustly modeled routinely. For instance, the clear concentration of mass loss along the coasts, mainly in the southeast and northwest, coincides with where detailed radar interferometry studies (4) have reported large ice flow speeds associated with outlet glaciers.

In the central high-elevation portions of Greenland, there is evidence for significant accumulation of ice mass, a result that was not clearly imaged by previous GRACE studies (17, 19, 22). However, in a combined inversion of GRACE and Global Positioning System data, the work by Wu et al. (35) did show some mass accumulation in central Greenland. Accumulation in the

continental interior is expected in a warming climate (3), and it has been observed also by satellite altimetry (1, 4, 5, 38). Recent modeling of Greenland's climate over the past 50 y (7) reveals that precipitation and runoff increased significantly beginning in 1996. Although the precise locations are unclear from these studies, between 2003 and 2008, large areas of Greenland's interior are thought to have gained mass (between 0 and 10 cm water equivalent per year, which is near the maximum that we recovered). Our observation of the interior mass accumulation is spatially very well-resolved, and this finding also represents a significant improvement over earlier attempts to localize this anticipated pattern from GRACE data alone.

The spatially well-resolved maps of Greenland's mass loss give us confidence to attempt extracting higher-resolution temporal variations of the geographic signal. When each year is examined in more detail (Fig. 3), the loci of largest mass loss move around Greenland with time. In 2003 and 2004, mass loss was concentrated along the entire eastern coast of Greenland. In 2005 and 2006, mass loss was reduced in the northeast but increased in the southeast. Meanwhile, mass loss began to increase along the northwest coast. From 2007 to 2010, mass loss further increased in northwest Greenland, whereas mass loss diminished in the southeast coast areas after 2008. Each year displays a region in the interior of Greenland with mass increases exceeding 5 cm/y (light blue), shifting slightly geographically from year to year.

Overall, the spatially shifting mass changes recovered by our method match well to remote-sensing observations. The increased mass loss in southeast Greenland first seen in 2005 coincides with accelerated flow observed in eastern outlet glaciers during that time (10). Increasing mass losses in northwest Greenland since 2006 are also seen in observations by radar interferometry and Global Positioning System (6, 22). The observed deceleration in mass loss in the southeast in 2009 and 2010 may be related to decreased glacier velocities in that region (39), although continued study is needed to substantiate this claim.

In addition, our results confirm the two large zones of melting (southeast and northwest coasts) seen in previous GRACE studies (17, 19, 20, 22). With our additional spatial detail, however, we observe more clearly the separation between these regions and their different mass changes over time. In our results, we observe larger magnitudes of surface density change than other GRACE studies, because the mass losses are concentrated on the coasts instead of being smoothed over larger areas. For this same reason, we observe fluctuating mass changes on Greenland's northeast coast, where other studies have not detected much variability. We also more clearly show the waxing and waning of mass in the southeast over the span of 8 individual years, with 2005 and 2006 exhibiting the largest mass losses compared with the others in the decade.

All together, our results show both the power of spatiospectrally concentrated Slepian localization methods in enhancing the signal-to-noise ratio for regional modeling, and of course, the benefits of long time series of time-variable gravimetry to examine the long-term mass flux over glaciated areas. As this kind of data (e.g., from the Gravity Recovery and Interior Laboratory (GRAIL) mission orbiting the moon or GRACE follow-on missions) continues to evolve with technology, so do the methods to study them. Pushing the envelope of the analysis will ensure that satellite gravity, even when other more direct observations should be lacking, will continue to play a major role in studying terrestrial, lunar, and planetary systems in the future.

ACKNOWLEDGMENTS. Our computer code is available online (www.frederik.net and http://polarice.princeton.edu) in both its general form and the application to Greenland. This work was supported by US National Science Foundation Grant EAR–1014606 (to F.J.S.).

1. Krabill W, et al. (2000) Greenland ice sheet: High-elevation balance and peripheral thinning. *Science* 289(5478):428–430.
2. Krabill W, et al. (2004) Greenland ice sheet: Increased coastal thinning. *Geophys Res Lett* 31:1–4.
3. Zwally HJ, et al. (2005) Mass changes of the Greenland and Antarctic ice sheets and shelves and contributions to sea-level rise: 1992–2002. *J Glaciol* 51:509–527.
4. Rignot E, Kanagaratnam P (2006) Changes in the velocity structure of the Greenland Ice Sheet. *Science* 311(5763):986–990.
5. Thomas R, Frederick E, Krabill W, Manizade S, Martin C (2006) Progressive increase in ice loss from Greenland. *Geophys Res Lett* 33:L10503.
6. Rignot E, Box JE, Burgess E, Hanna E (2008) Mass balance of the Greenland ice sheet from 1958 to 2007. *Geophys Res Lett* 35:L20502.
7. van den Broeke M, et al. (2009) Partitioning recent Greenland mass loss. *Science* 326 (5955):984–986.
8. Joughin I, Abdalati W, Fahnestock M (2004) Large fluctuations in speed on Greenland's Jakobshavn Isbrae glacier. *Nature* 432(7017):608–610.
9. Luckman A, Murray T (2005) Seasonal variation in velocity before retreat of Jakobshavn Isbræ, Greenland. *Geophys Res Lett* 32:L08501.
10. Luckman A, Murray T, de Lange R, Hanna E (2006) Rapid and synchronous ice-dynamic changes in East Greenland. *Geophys Res Lett* 33:L03503.
11. Howat IM, Joughin I, Scambos TA (2007) Rapid changes in ice discharge from Greenland outlet glaciers. *Science* 315(5818):1559–1561.
12. Joughin I, et al. (2008) Seasonal speedup along the western flank of the Greenland Ice Sheet. *Science* 320(5877):781–783.
13. Chen JL, Wilson CR, Tapley BD (2006) Satellite gravity measurements confirm accelerated melting of Greenland ice sheet. *Science* 313(5795):1958–1960.
14. Luthcke SB, et al. (2006) Monthly spherical harmonic gravity field solutions determined from GRACE inter-satellite range-rate data alone. *Geophys Res Lett* 33:L02402.
15. Velicogna I, Wahr J (2006) Acceleration of Greenland ice mass loss in spring 2004. *Nature* 443(7109):329–331.
16. Ramillien G, et al. (2006) Interannual variations of the mass balance of the Antarctica and Greenland ice sheets from GRACE. *Global Planet Change* 53:198–208.
17. Wouters B, Chambers D, Schrama EJO (2008) GRACE observes small-scale mass loss in Greenland. *Geophys Res Lett* 35:L20501.
18. Velicogna I (2009) Increasing rates of ice mass loss from the Greenland and Antarctic ice sheets revealed by GRACE. *Geophys Res Lett* 36:L19503.
19. Chen JL, Wilson CR, Tapley BD (2011) Interannual variability of Greenland ice losses from satellite gravimetry. *J Geophys Res* 116:B07406.
20. Schrama EJO, Wouters B (2011) Revisiting Greenland ice sheet mass loss observed by GRACE. *J Geophys Res* 116:B02407.
21. Swenson S, Wahr J (2006) Post-processing removal of correlated errors in GRACE data. *Geophys Res Lett* 33:L08402.
22. Kahn SA, Wahr J, Bevis M, Velicogna I, Kendrick E (2010) Spread of ice mass loss into northwest Greenland observed by GRACE and GPS. *Geophys Res Lett* 37:L06501.
23. Simons FJ, Dahlen FA, Wieczorek MA (2006) Spatiospectral concentration on a sphere. *SIAM Rev Soc Ind Appl Math* 48:504–536.
24. Simons FJ, Dahlen FA (2006) Spherical Slepian functions and the polar gap in geodesy. *Geophys J Int* 166:1039–1061.
25. Dahlen FA, Simons FJ (2008) Spectral estimation on a sphere in geophysics and cosmology. *Geophys J Int* 174:774–807.
26. Simons FJ, Dahlen FA (2007) A spatiospectral localization approach to estimating potential fields on the surface of a sphere from noisy, incomplete data taken at satellite altitudes. *Proc SPIE* 6701:670117.
27. Swenson S, Wahr J, Milly PCD (2003) Estimated accuracies of regional water storage variations inferred from the Gravity Recovery and Climate Experiment (GRACE). *Water Resour Res* 39:1–11.
28. Slepian D (1983) Some comments on Fourier analysis, uncertainty, and modeling. *SIAM Rev Soc Ind Appl Math* 25:379–393.
29. Cheng M, Tapley BD (2004) Variations in the Earth's oblateness during the past 28 years. *J Geophys Res* 109:B09402.
30. Swenson S, Chambers D, Wahr J (2008) Estimating geocenter variations from a combination of GRACE and ocean model output. *J Geophys Res* 113:B08410.
31. Wahr J, Molenaar M, Bryan F (1998) Time variability of the Earth's gravity field: Hydrological and oceanic effects and their possible detection using GRACE. *J Geophys Res* 103:30205–30229.
32. Le Meur E, Huybrechts P (2001) A model computation of the temporal changes of suface gravity and geoidal signal induced by the evolving Greenland ice sheet. *Geophys J Int* 145:835–849.
33. Wieczorek MA, Simons FJ (2005) Localized spectral analysis on the sphere. *Geophys J Int* 162:655–675.
34. Paulson A, Zhong S, Wahr J (2007) Inference of mantle viscosity from GRACE and relative sea level data. *Geophys J Int* 171:497–508.
35. Wu X, et al. (2010) Simultaneous estimation of global present-day water transport and glacial isostatic adjustment. *Nat Geosci* 3:642–646.
36. Sasgen I, et al. (2012) Timing and origin of recent regional ice-mass loss in Greenland. *Earth Planet Sci Lett* 333–334:293–303.
37. Sørensen LS, et al. (2011) Mass balance of the Greenland ice sheet (2003–2008) from ICESat data—the impact of interpolation, sampling and firn density. *Cryosphere* 5:173–186.
38. Johannessen OM, Khvorostovsky K, Miles MW, Bobylev LP (2005) Recent ice-sheet growth in the interior of Greenland. *Science* 310(5750):1013–1016.
39. Murray T, et al. (2010) Ocean regulation hypothesis for glacier dynamics in southeast Greenland and implications for ice sheet mass changes. *J Geophys Res* 115:F03026.

Supporting Information

Harig and Simons 10.1073/pnas.1206785109

SI Text

Determination of Noise. Gravity Recovery and Climate Experiment (GRACE) data are released as spherical harmonic coefficients along with calibrated errors that represent the diagonal elements of the covariance matrix of the estimated global monthly solutions. It is known that these calibrated errors underestimate the variance in GRACE solutions (1) and that monthly solutions are dominated by north–south trending linear stripe anomalies (2). Thus, many studies estimate their own uncertainty for their modeling (3) and attempt to remove estimated noise components (2, 4).

In practice, there is little reason to think that time-variable geopotential signals are best estimated from basis functions that spread their energy over the entire globe. For instance, processes that act in different locations at different times (e.g., monsoons) could easily display competing effects in the same spherical harmonic coefficient. Thus, in our determination of noise specifically over Greenland, we estimate signal and noise in the Slepian basis to avoid contamination from other regions. However, to illustrate the importance of estimating the noise covariance and accounting for it in the subsequent analysis, the global spherical harmonic analysis performed here provides a convenient example. This method of estimating the noise in GRACE data from the spherical harmonic coefficients was first used in the work by Wahr et al. (3) and has subsequently been used in a great many of GRACE studies.

Here, we examine each spherical harmonic coefficient individually as it varies over time, and we find a least squares estimate of a linear term and a seasonal term with a 365-d period. We consider this fit to be an estimate of the signal contained in the GRACE data, and the residuals form a conservative estimate of the noise. Fig. S1, which examines the coefficients spectrally, shows the results of this procedure. Fig. S1*A* shows a single monthly solution of GRACE data for February of 2010. Fig. S1*C* shows the prediction of the signal component for this month. Fig. S1*D* shows the residual after subtracting the signal from the data. Generally, the prediction is dominated by energy in coefficients with degrees less than 30. Meanwhile, the residual has some energy at low-degree coefficients, but it is mainly comprised of energy in coefficients where the order m (and degree l) is $-30 \gtrsim m \gtrsim 30$. This result corresponds to the higher-frequency north–south-oriented stripes commonly observed. Finally, Fig. S1*B* shows the SDs of these residual coefficients over all of the months considered. We have made the implicit assumption that the noisy stripes seen in GRACE monthly data are related to the satellite orbit characteristics specific to each month considered, and therefore, these stripes should not have a coherent secular expression over time.

Covariance of the Noise. We use the spherical harmonic coefficient residuals from each month to construct a covariance matrix (Fig. S2, shown as a correlation matrix). The residual correlation matrix shows many off-diagonal terms with large correlations. This finding is contrary to what is normally assumed by other works, which examine only the diagonal elements of this matrix (the variance) and assume that the off-diagonal terms are zero.

These large covariance terms make important contributions to the observed spatial covariance on the sphere. In Fig. S3, we show the difference in spatial covariance when the full spectral covariance matrix or only the variance (its diagonal elements) is being used. We consider the covariance between a point in central Greenland and all of the other points on the Earth, and we do the same with a point in western Antarctica.

Additionally, in Fig. S4, we show how our spatial variance compares with the calibrated errors distributed with the monthly geopotential solutions. Most notably, our spatial variance has significant longitudinal dependence compared with the calibrated errors, while also displaying somewhat higher values of SD than the calibrated errors. It is clear that, without the use of the full covariance matrix, estimates of the error in mass change results may be inaccurate. By taking a conservative estimate of the full noise covariance of the data into account, we can have high confidence in our mass estimates compared with the results derived from other techniques.

Spherical Slepian Basis. Given that (*i*) time-variable gravity signals often originate in specific regions of interest (*ii*), our data are discreetly measured and therefore, have a band limit, and (*iii*) we may wish to exclude some portion of the spectrum where the error terms are expected to dominate, then we desire an orthogonal basis on the sphere that is both optimally concentrated in our spatial region of interest and band-limited to a chosen degree. For this purpose, we use the spherical analog to the classic Slepian concentration problem (5–8) and define a new set of basis functions (Eq. **S1**):

$$g_\alpha(\hat{\mathbf{r}}) = \sum_{l=0}^{L} \sum_{m=-l}^{l} g_{\alpha,lm} Y_{lm}(\hat{\mathbf{r}}), \quad g_{\alpha,lm} = \int_\Omega g_\alpha(\hat{\mathbf{r}}) Y_{lm}(\hat{\mathbf{r}}) d\Omega. \quad \textbf{[S1]}$$

These functions maximize their energy within our region of interest R following (Eq. **S2**)

$$\lambda = \frac{\int_R g_\alpha^2(\hat{\mathbf{r}}) d\Omega}{\int_\Omega g_\alpha^2(\hat{\mathbf{r}}) d\Omega} = \text{maximum}, \quad \textbf{[S2]}$$

where $1 > \lambda > 0$. The Slepian coefficients, $g_{\alpha,lm}$, are found by solving the eigenvalue equation (Eq. **S3**)

$$\sum_{l'=0}^{L} \sum_{m'=-l'}^{l'} D_{lm,l'm'} g_{l'm'} = \lambda g_{lm}, \quad \textbf{[S3]}$$

where the elements of $D_{lm,l'm'}$ are products of spherical harmonics integrated over the region R (Eq. **S4**):

$$\int_R Y_{lm} Y_{l'm'} \, d\Omega = D_{lm,l'm'}. \quad \textbf{[S4]}$$

The Slepian basis is an ideal tool to conduct estimation problems that are linear or quadratic in the data (8, 9). The data can now be projected into this basis as (Eq. **S5**)

$$d(\hat{\mathbf{r}}) = \sum_{\alpha=1}^{(L+1)^2} d_\alpha g_\alpha(\hat{\mathbf{r}}) = \sum_{l=0}^{L} \sum_{m=-l}^{l} d_{\alpha,lm} Y_{lm}(\hat{\mathbf{r}}) \quad \textbf{[S5]}$$

and by using a truncated sum up to the spherical Shannon number (Eq. **S6**),

$$N = (L+1)^2 \frac{A}{4\pi}, \quad \textbf{[S6]}$$

where $A/4\pi$ is the fractional area of localization to R, we can sparsely approximate the data, yet with very good reconstruction properties within the region (10) (**S7**):

$$d(\hat{\mathbf{r}}) \approx \sum_{\alpha=1}^{N} d_\alpha g_\alpha(\hat{\mathbf{r}}) \quad \text{for} \quad \hat{\mathbf{r}} \in R. \qquad \text{[S7]}$$

This procedure is analogous to taking a truncated sum of the singular-value decomposition of an ill-posed inverse problem (10). Because the illposedness is, in part, derived from the focus on the limit area of interest, our procedure in effect determines the singular vectors of the inverse problem from the outset based on purely geometric considerations, which is efficient.

We solve for a Slepian basis for Greenland (Fig. S5) up to the same degree and order of the available GRACE data (thus, the bandwidth $L = 60$). We use the coastlines of Greenland and extend them by 0.5° to create the region of concentration R. With truncation at the Shannon number N, the basis has 20 Slepian functions localized to the region, with the 12th best function (Fig. S5) still concentrated to $\lambda = 86.9\%$.

The Slepian functions are smoothly varying across the land–ocean boundary, and as a result, they can have reduced sensitivity near this boundary. This result is why we extended the concentration region by buffering away from the coastlines. The size of the buffer zone was based on experiments to recover a synthetic mass trend placed uniformly on Greenland's landmass (Fig. S6). In Fig. S6*A*, we show the results of an experiment where a uniform synthetic signal is placed over Greenland, and we attempt to recover this trend. To replicate the experimental conditions faced by the researchers on the ground, we add synthetic realizations of the noise generated from our empirical covariance matrix to this synthetic signal. The signal is best recovered when the region of localization is extended away from the coastlines by 0.5°. This buffer region allows us to better measure mass changes near the coastlines of Greenland, but it is small enough to eliminate influence by mass changes outside of Greenland, such as in Iceland or Svalbard. In Fig. S6*B*, we show how the actual recovered mass trends over Greenland vary depending on the bandwidth and buffer (i.e., region) chosen. Roughly the same trend is recoverable for a broad combination of bandwidth and region buffer; however the lower bandwidths will have reduced spatial sensitivity around Greenland.

Analysis in the Slepian Basis. We project each monthly GRACE field, which we convert to surface density, into the Slepian basis for Greenland, which results in a time series for each Slepian expansion coefficient. For each of our 20 Slepian coefficients, we fit a first-, second-, or third-order polynomial to the time series in addition to a 365-d period sinusoidal function, depending on whether each additional polynomial term passes an F test for significance. These quadratic and cubic terms represent the interannual changes in the GRACE data over the data time span. Examples of these fits are shown in Fig. S7. Here, we show the time series of some coefficients and their best-fitting functions, where the fitted annual periodic function has been subtracted. Some time series, such as for $\alpha = 20$, are best represented by a higher-order polynomial, whereas others, such as $\alpha = 11$, are fit by a linear function, because higher-order terms do not significantly reduce variance.

The mass change for an average year, shown in Fig. S8, is found by taking the total estimated mass change from 2003 to 2010 and dividing by time considered. Most of the mass change of this period projects into the first five Slepian functions; however, the remaining 15 functions of the basis are also important to fully capture the spatial pattern of mass change, even if their mass integrals do not form a large part of the total.

After fitting estimated signals in the Slepian domain, the monthly residuals can be used to form an empirical covariance matrix for the Slepian functions (Fig. S2*B*). This information not only gives us estimates for the uncertainty of the signal estimates for each Slepian function but also allows us to determine the overall trend uncertainty for all of Greenland by combining the variance and covariance in error propagation. Using the full covariance information allows us to have high confidence in our trend estimation, more than we felt comfortable with in previous work.

Finally, we can examine the time series for the three most-contributing Slepian functions, which Fig. S9 expresses as the integral of the product of the expansion coefficient and the function. It is clear from this behavior function that the mass signal trends can be well-estimated relative to the variance seen from month to month. The Slepian functions significantly enhance signal to noise within the region of interest compared with traditional spherical harmonics, which further validates our approach.

1. Horwath M, Dietrich R (2006) Errors of regional mass variations inferred from GRACE monthly solutions. *Geophys Res Lett* 33:L07502.
2. Swenson S, Wahr J (2006) Post-processing removal of correlated errors in GRACE data. *Geophys Res Lett* 33:L08402.
3. Wahr J, Swenson S, Velicogna I (2006) Accuracy of GRACE mass estimates. *Geophys Res Lett* 33:L06401.
4. Chen JL, Wilson CR, Tapley BD, Blankenship D, Young D (2008) Antarctic regional ice loss rates from GRACE. *Earth Planet Sci Lett* 266:140–148.
5. Slepian D (1983) Some comments on Fourier analysis, uncertainty, and modeling. *SIAM Rev Soc Ind Appl Math* 25:379–393.
6. Wieczorek MA, Simons FJ (2005) Localized spectral analysis on the sphere. *Geophys J Int* 162:655–675.
7. Simons FJ, Dahlen FA, Wieczorek MA (2006) Spatiospectral concentration on a sphere. *SIAM Rev Soc Ind Appl Math* 48:504–536.
8. Simons FJ, Dahlen FA (2006) Spherical Slepian functions and the polar gap in geodesy. *Geophys J Int* 166:1039–1061.
9. Dahlen FA, Simons FJ (2008) Spectral estimation on a sphere in geophysics and cosmology. *Geophys J Int* 174:774–807.
10. Simons FJ (2010) *Handbook of Geomathematics*, eds Freeden W, Nashed MZ, Sonar T (Springer, Berlin), pp 891–923.

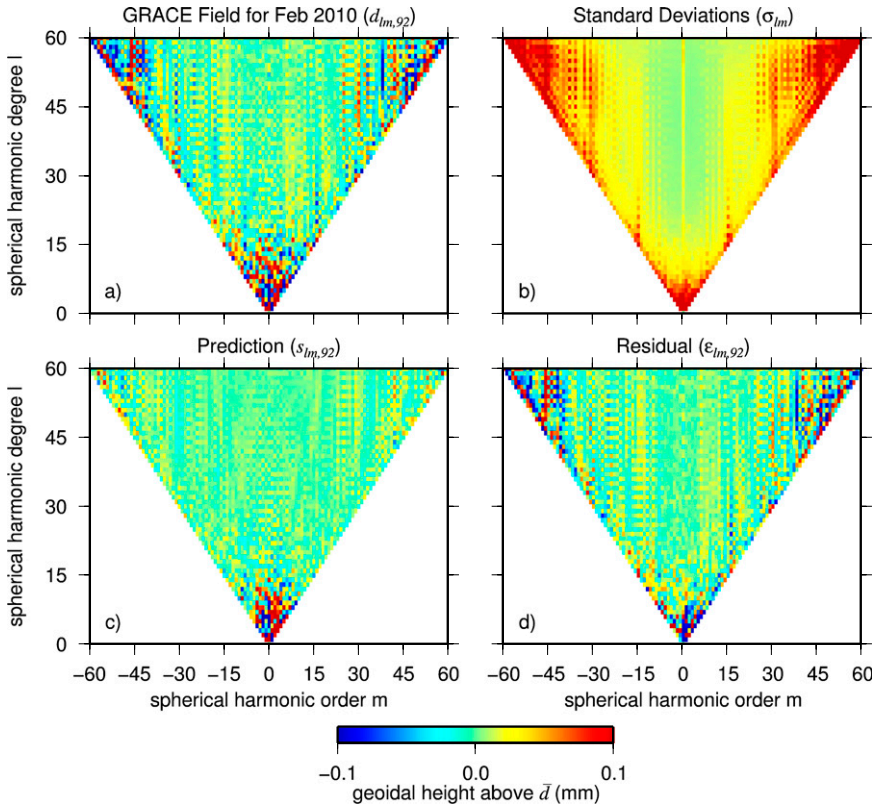

Fig. S1. Ordered maps of various spherical harmonic coefficients. (*A*) The geoidal coefficients ($d_{lm,92}$) of GRACE data from February of 2010 after the average of all data months has been removed. (*B*) SDs ($\sigma_{lm} = [1/M\sum_{n=1}^{M} d_{lm,n}]^{1/2}$ for months $n = 1, \ldots, M$, where $n = 92$ stands for February of 2010) of the residuals as estimated by subtracting the least squares fits comprising a linear and two seasonal terms with periods 365 and 181 d from each time series of geoidal spherical harmonic coefficients and computing the covariance of the results. (*C*) The predicted geoidal coefficients ($s_{lm,92}$) from the least squares model fit as described before in *B*. (*D*) The residual geoidal coefficients ($\epsilon_{lm,92} = d_{lm,92} - s_{lm,92}$) were determined by subtracting the predicted coefficients (*C*) from the GRACE geoidal field (*A*).

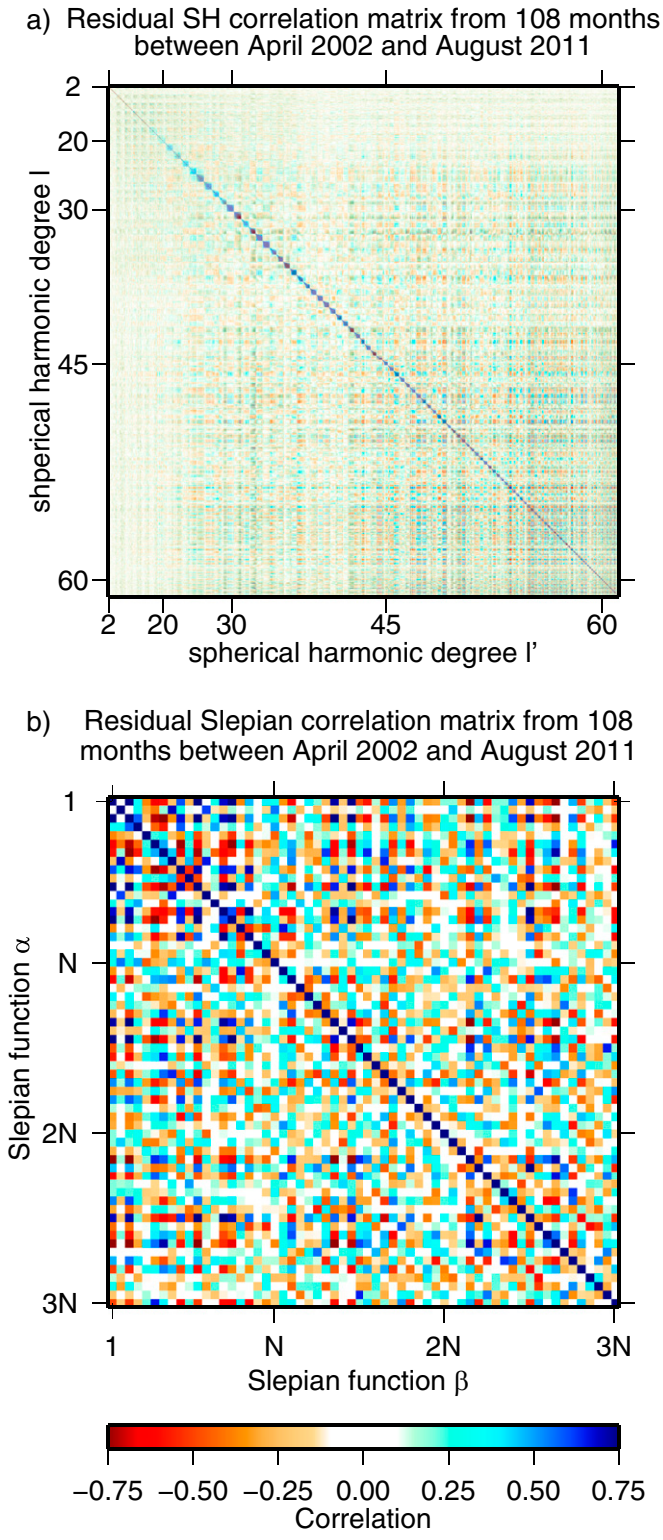

Fig. S2. Correlation matrices for spherical harmonic and Slepian coefficients created from the residuals of 108 mo from April of 2002 to August of 2011. (*A*) Correlation between spherical harmonic coefficients derived from the spectral covariance cov[ε_{lm}, $\varepsilon_{l'm'}$]. (*B*) Correlation between Slepian function coefficients for a basis for Greenland with a region buffer of 0.5° and a bandwidth $L = 60$. The rounded Shannon number is $n = 20$.

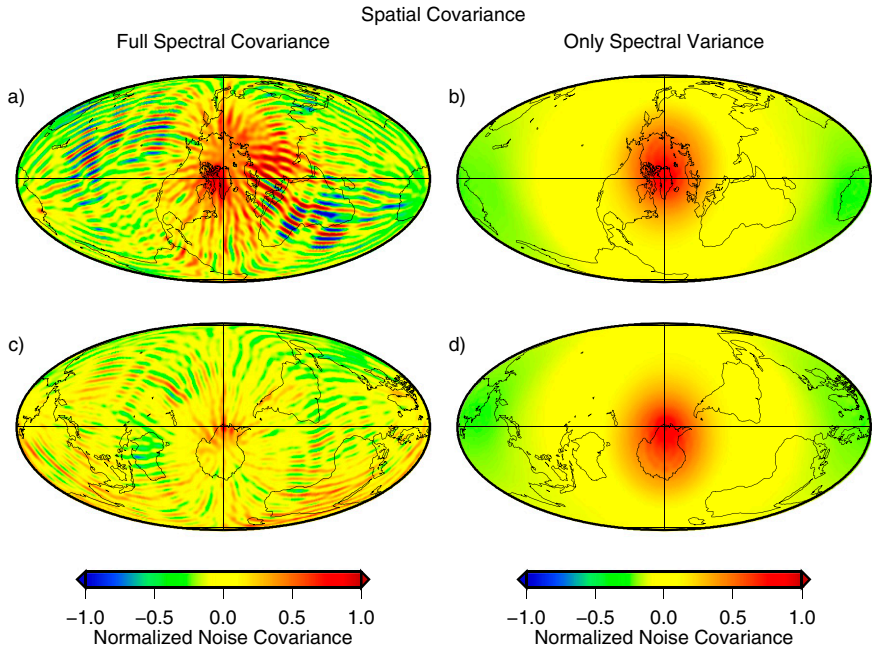

Fig. S3. Spatial covariance plots of residuals, cov[ε_r, $\varepsilon_{r'}$]. Fields have been rotated, and therefore, the central cross denotes the point r with which all of the other points r′ covary. In *A* and *C*, the full spectral covariance matrix is used. *B* and *D* use only the spectral variance and the diagonal elements of covariance matrix. (*A* and *B*) The covariance of a point in Greenland with the rest of the Earth. (*C* and *D*) Covariance of a point in western Antarctica with the rest of the globe.

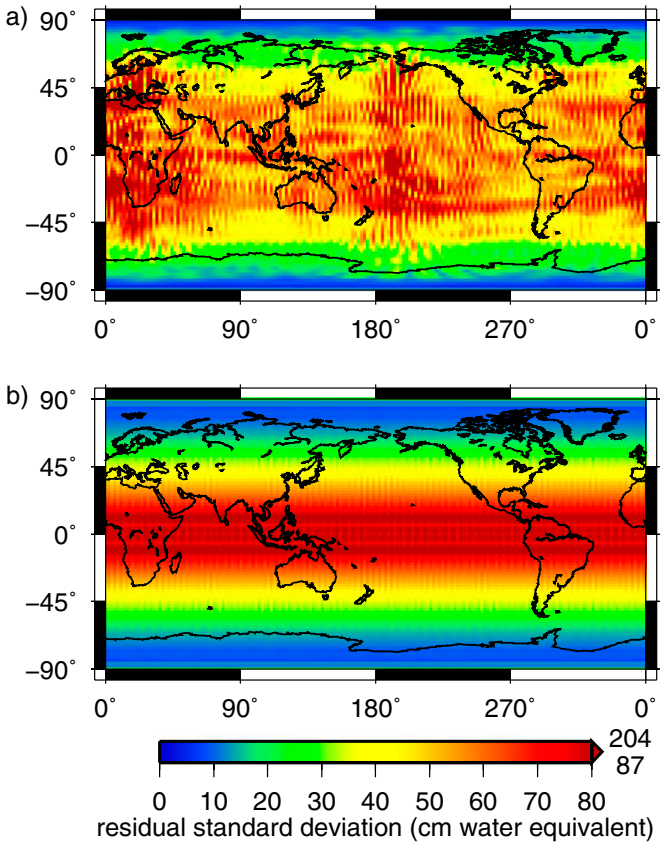

Fig. S4. (*A*) Spatial SD from our full spectral estimated covariance matrix, and (*B*) SD using only the spectral variance (diagonal) terms of the covariance matrix (off-diagonal terms are set to zero). Both plots are saturated at 80 cm water equivalent, but *A* and *B* have the denoted maximums of 204 and 87 cm, respectively.

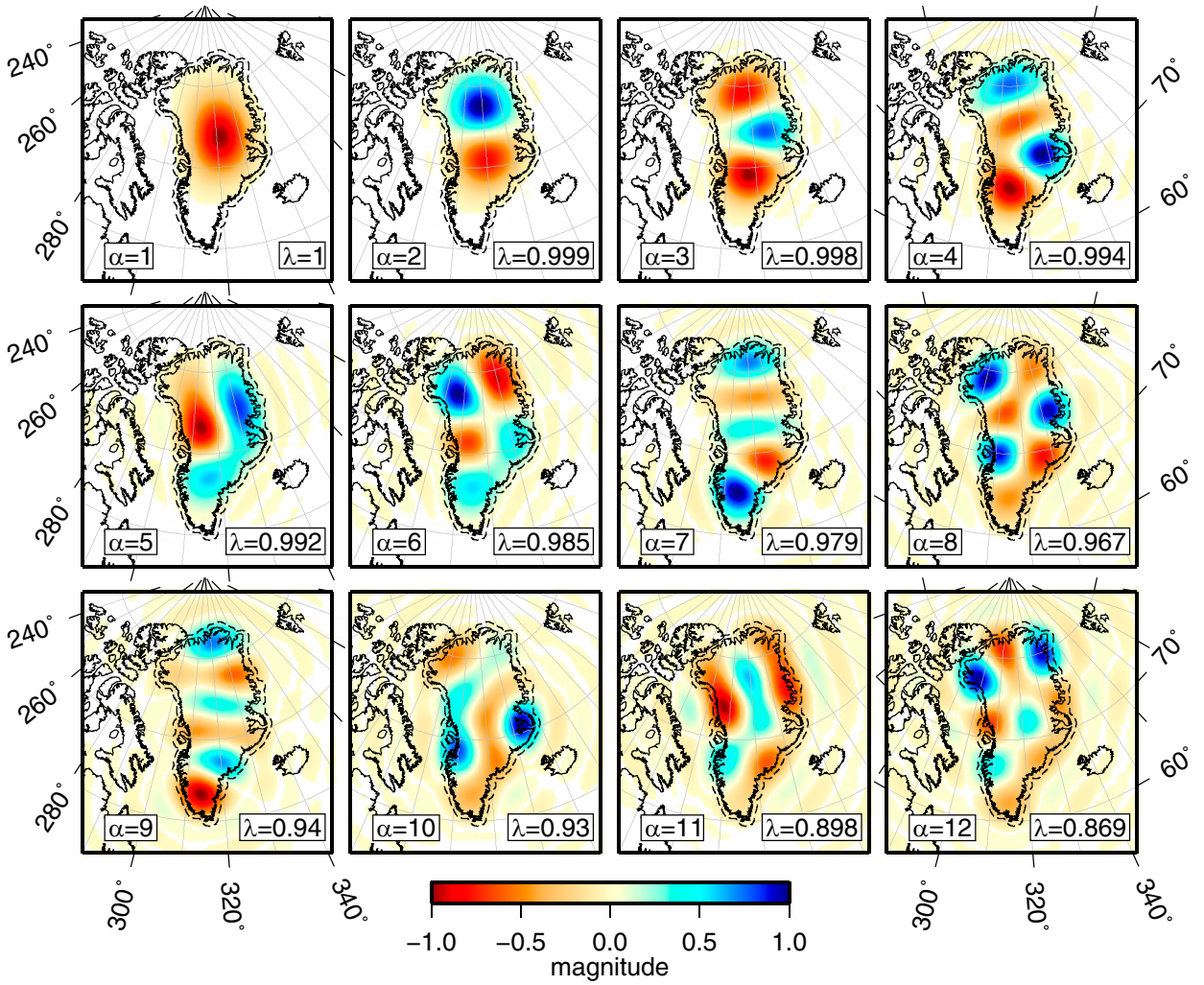

Fig. S5. Slepian eigenfunctions g_1, g_2, ..., g_{12} that are optimally concentrated within a region buffering Greenland by 0.5°. The dashed lines indicate the regions of concentration. Functions are band-limited to $L = 60$ and scaled to unit magnitude. The parameter α denotes the eigenfunction that is shown. The parameter λ is the corresponding eigenvalue for each function, indicating the amount of concentration. Magnitude values with absolute values that are smaller than 0.01 are left white.

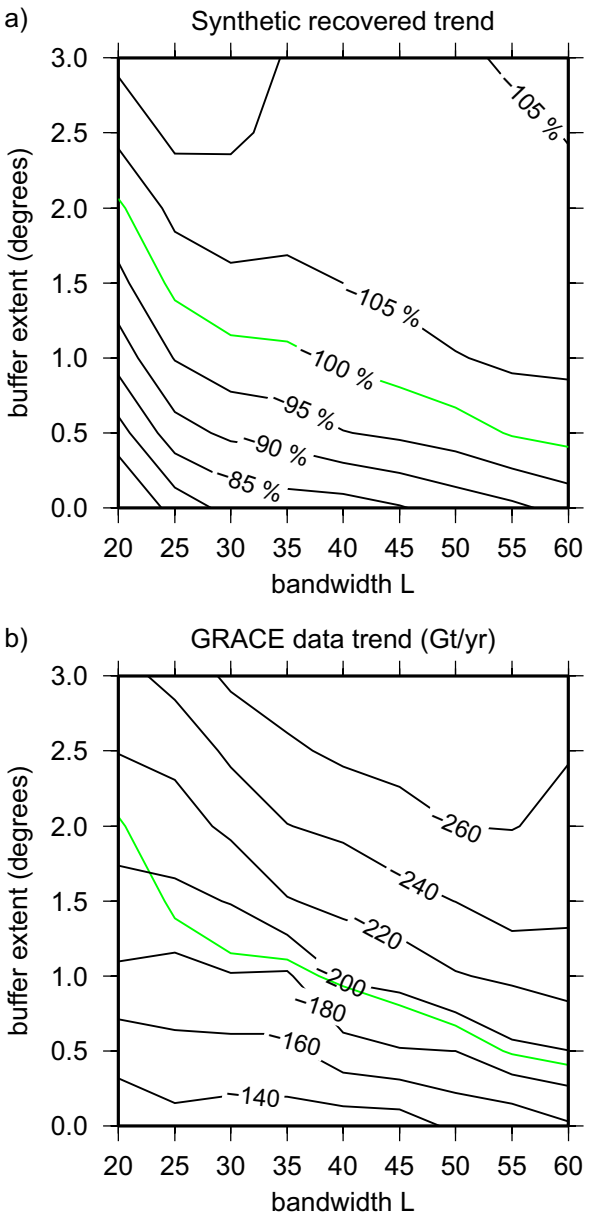

Fig. S6. The results of synthetic experiments to examine how recovered trends vary for different bandwidths (*L*) and different region buffers. (*A*) We place a uniform mass loss trend over the landmass of Greenland. To this trend, at each month, we add a realization of the noise from our residual covariance matrix. We then attempt to recover this trend for different bases over Greenland and report the normalized trend. (*B*) For the same bases, we report the trend recovered from the actual GRACE data in gigatons per year. Also drawn is the 100% recovery contour (*A*). We use this synthetic experiment to inform our preferred choice of a 0.5° buffer around Greenland.

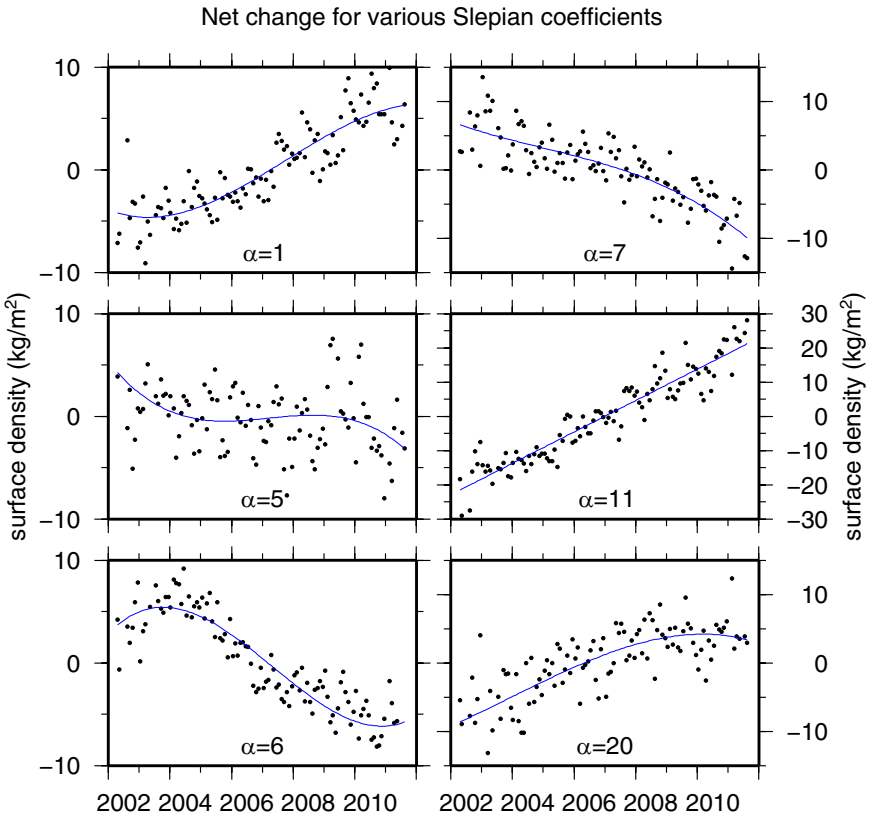

Fig. S7. Time series of various (α = 1, 5, 6, 7, 11, 20) Slepian coefficients and their best-fit polynomial (blue lines). Each coefficient is fit by an annual periodic and linear function as well as quadratic and cubic polynomial terms if those terms pass an *F* test for variance reduction. Shown here are the coefficient and fitted function values with the annual periodic function subtracted from both. The mean is removed from each time series.

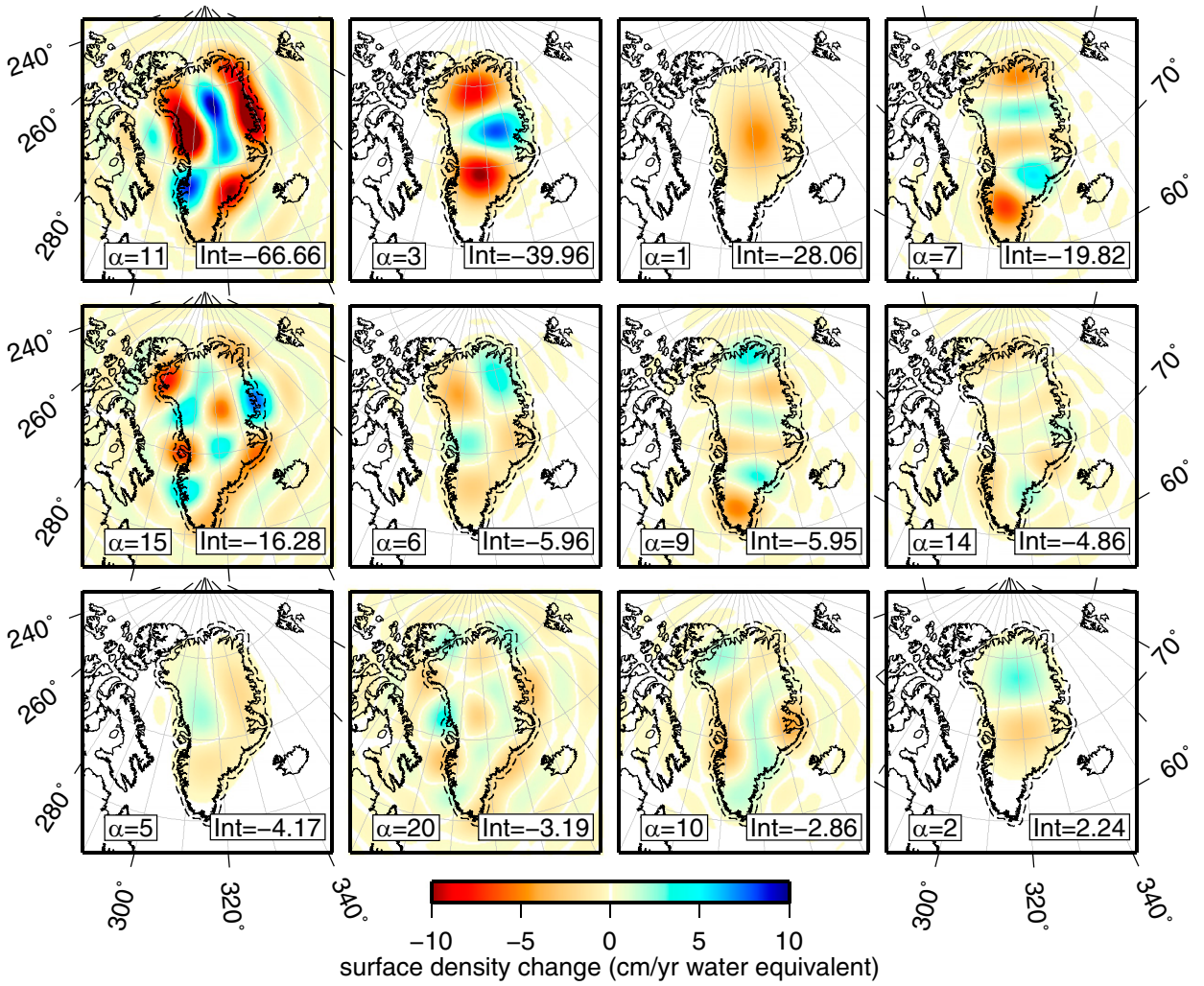

Fig. S8. Predicted GRACE annual mass change in the Slepian basis for each of the first 12 eigenfunctions. Each eigenfunction, denoted by its index α, is scaled by the total change in that coefficient from January of 2003 to November of 2011 divided by the time span (years) expressed as the centimeter per year water equivalent of surface density. Thus, this result represents the mass change for an average year during this time span. The variable Int displays the integral of each function in the concentration region within the dashed line expressed as the mass change rate of gigatons per year. Surface density change of absolute value smaller than 0.1 cm/y is left white.

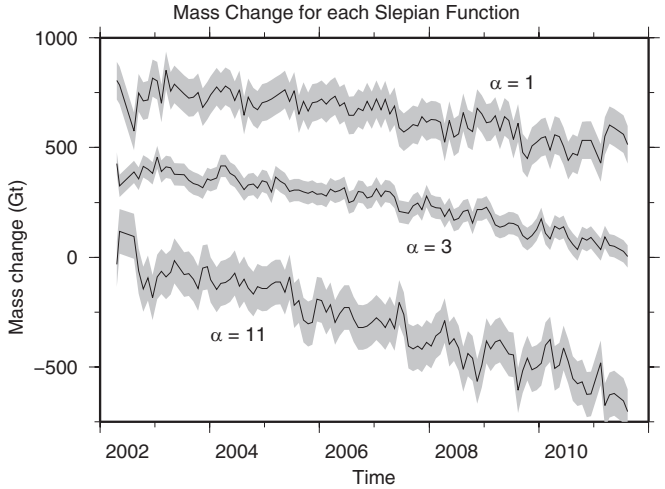

Fig. S9. Mass change in gigatons for the three most significant Slepian function terms (α = 1, 3, 11), which contribute more than 70% of total mass change over the data time span. Monthly data are drawn as the solid black lines, whereas the 2σ uncertainty envelopes are drawn in gray. Each function has a mean of zero but has been offset from zero for clarity.